

Supporting Information:
Polymorphism in $M(\text{H}_2\text{PO}_2)_3$ ($M = \text{V}, \text{Al}, \text{Ga}$) compounds
with the perovskite-related ReO_3 structure.

E-mail:

Hayden A. Evans,^{ab‡} Zeyu Deng,^{cd‡} Ines E. Collings,^e Yue Wu,^c Jessica L. Andrews,^a Kartik Pilar,^b Joshua M. Tuffnell,^f Guang Wu,^a John Wang,^c Siân E. Dutton,^f Paul D. Bristowe,^d Ram Seshadri,^{abg} and Anthony K. Cheetham,^{bcd}

[‡] *These authors contributed equally to this work.* ^a*Department of Chemistry and Biochemistry, University of California, Santa Barbara, California 93106 United States.* ^b*Materials Research Laboratory, University of California, Santa Barbara, California 93106 United States* ^c*Department of Materials Science and Engineering, National University of Singapore, Singapore 117575, Singapore* ^d*Department of Materials Science and Metallurgy, University of Cambridge, 27 Charles Babbage Rd, CB3 0FS Cambridge, UK* ^e*European Synchrotron Radiation Facility, 71 avenue des Martyrs, 38000 Grenoble, France* ^f*Cavendish Laboratory, Department of Physics, University of Cambridge, JJ Thomson Avenue, Cambridge CB3 0HE, United Kingdom* ^g*Materials Department, University of California, Santa Barbara, California 93106 United States*

Experimental Information

Bulk β -V(H₂PO₂)₃ was prepared with a modified procedure from Maouel *et al.*¹ 0.100 g (0.550 mmol) V₂O₅ (Strem 98%), and 1.426 g (10.8 mmol) H₃PO₂ aqueous solution (Spectrum, 50% wt/wt) were combined in a teflon lined Parr vessel and heated from room temperature to 150°C over the course of 24 hours (\approx 0.1°C/min), held at 150°C for 48 hours, and then cooled from 150°C to room temperature over the course of 24 hours (\approx 0.1°C/min). A solid green *puck* of β -V(H₂PO₂)₃ was isolated from a green mother liquor via vacuum filtration. This puck was broken up, washed with copious amounts of H₂O then ethanol, and lastly vacuum dried at 60°C overnight. For small crystals of β -V(H₂PO₂)₃, the same procedure can be followed with the addition of 0.180 g (2.43 mmol) Li₂CO₃ (Sigma-Aldrich, 99.0%) to the V₂O₅ and H₃PO₂ solution. This should be allowed to off-gas CO₂ before sealing the Parr vessel.

A sample of Al(H₂PO₂)₃, that contained both α - and γ -Al(H₂PO₂)₃, was prepared as follows: 0.124 g (0.61 mmol) Al(O-*i*-Pr)₃ and 1.426 g (10.8 mmol) H₃PO₂ aqueous solution (Spectrum, 50% wt/wt) were combined in a teflon lined Parr vessel and placed into a preheated oven at 150°C oven for 24 hours. This Parr vessel was then removed from the oven, and air cooled to room temperature. The white colored product was then isolated from a clear/grey mother liquor via vacuum filtration, washed with copious amounts of H₂O then ethanol, and vacuum dried at 60°C overnight. We observed no difference in product composition if a longer heating profile, like that used for β -V(H₂PO₂)₃, was implemented. The final white colored product had larger cube-habit crystals that could be separated with visual assistance from an optical microscope. These larger cube-habit crystals were α -Al(H₂PO₂)₃, with the remainder of the white powder being small crystals of γ -Al(H₂PO₂)₃. A pure γ Al(H₂PO₂)₃ sample was prepared by using 0.055 g (0.53 mmol) γ -Al₂O₃ (Strem, 97%) instead of Al(O-*i*-Pr)₃ following the same procedure. Corundum Al₂O₃ cannot be used instead of γ -Al₂O₃, as corundum Al₂O₃ will not react under these conditions. For small crystals of γ -Al(H₂PO₂)₃, the procedure using γ -Al₂O₃ can be followed,

with the addition of 0.180 g (2.43 mmol) Li_2CO_3 (Sigma-Aldrich, 99.0%) to the $\gamma\text{-Al}_2\text{O}_3$ and H_3PO_2 solution. This mixture should be allowed to off-gas CO_2 before sealing the Parr vessel.

A phase pure sample of $\alpha\text{-Ga}(\text{H}_2\text{PO}_2)_3$ was prepared by combining 0.09 g (0.48 mmol) Ga_2O_3 and 1.426 g (10.8 mmol) H_3PO_2 aqueous solution (Spectrum, 50% wt/wt) in a teflon lined Parr vessel, heating for 24 hours in a preheated 150°C oven, and removed to air cool. This product, which produced $1\text{ mm}\times 1\text{ mm}\times 1\text{ mm}$ clear crystals of $\alpha\text{-Ga}(\text{H}_2\text{PO}_2)_3$, was washed with H_2O then ethanol, and vacuum dried at 60°C overnight.

Single crystal X-ray diffraction data was collected on a Bruker KAPPA APEX II diffractometer equipped with an APEX II CCD detector using a TRIUMPH monochromator with a $\text{Mo K}\alpha$ X-ray source ($\lambda = 0.71073\text{ \AA}$). The crystals were mounted on a cryoloop under Paratone-N oil. Absorption correction of the data was carried out using the multi-scan method as implemented in SADABS.² Subsequent calculations were carried out using SHELXTL.³ Structure determination was done using intrinsic methods. Structure solution, refinement, and creation of publication data was performed using SHELXTL. Crystal structures were visualized using the VESTA software suite.⁴

High-pressure SCXRD data were measured for $\text{Ga}(\text{H}_2\text{PO}_3)_2$ at the ID15B beamline of the European Synchrotron Radiation Facility, Grenoble up to 2.2 GPa with Daphne 7373 oil as the pressure-transmitting medium (PTM) and up to 4.8 GPa with neon as the PTM at room temperature, using monochromatic X-ray radiation ($\lambda = 0.41112$).⁵ Membrane driven LeToullec type diamond anvil cells (DACs) were used, equipped with Boehler-Almax anvils. Stainless steel was used as the gasket material, Daphne 7373 oil was loaded as the PTM, as it is non-penetrating and non-reactive,⁶ while neon was used in the second loading to try and induce neon entry into the framework pores upon compression. Diffraction patterns were collected with a Mar555 flat panel detector. For the single-crystal data collection, steps of 0.5° oscillation were used over a total ω -scan range of 76° about the vertical axis. The single crystals were centred on the rotation axis using their absorption

profile from the X-rays. Lattice parameter determination and integration of the reflection intensities were performed using the *CrysAlisPro* software suite.⁷ Two different crystals were loaded in the gasket chamber in order to increase the chances of solving potential high-pressure phases. The single crystal structures were refined using *shelxL*, and structure solution was performed with *shelxT*, within *shelXle*.⁸⁻¹⁰ The pressures were measured using the ruby fluorescence method before and after each diffraction measurement. The reversibility of the phase transition was checked by measuring single-crystal data upon decompression.

Void space calculations were performed with the Mercury Software suite. A grid spacing of 0.1 Å was used for all calculations as probe radius was varied.¹¹

Room temperature powder X-ray diffraction was performed on a Panalytical Empyrean Powder Diffractometer (Bragg-Brentano HD module, no monochromator) equipped with a Cu source $\lambda = 1.5418$ Å. Rietveld refinements were performed in the TOPAS software suite.¹² Variable temperature measurements $T = 12$ –300 K were collected on a Bruker D8 Advance diffractometer, using an Oxford Cryosystems PheniX stage from $2\theta = 5^\circ$ – 120° with step size of $2\theta = 0.0204^\circ$ and Cu $K\alpha$ sources, $\lambda = 1.54$ Å.

Thermogravimetric analysis (TGA) on all compounds was conducted using a TA Instruments Discovery instrument. A rate of 25 cm³/min dry nitrogen purge was employed with a temperature ramp rate of 10°C/min. The maximum temperature of the experiment was 900°C.

NMR experiments were done using a Bruker Avance 800 MHz NMR spectrometer with a solid-state 2.5 mm HX double resonance magic angle spinning (MAS) probe. Ga(H₂PO₂)₃ was packed in a zirconia rotor and spun at 35 kHz. Single pulse experiments (SPE) were carried out for ¹H and ³¹P nuclei with resonant frequencies of 800 and 324 MHz, respectively. Additionally, a ³¹P spectrum was obtained with ¹H decoupling to minimize ¹H-³¹P dipole-dipole interactions to achieve narrower ³¹P linewidths. An 8 μs and 1.9 μs 90° pulse was used to excite ¹H and ³¹P nuclei, respectively, with an 80 s and 800 s recycle delay

between ^1H and ^{31}P scans. ^{31}P T_1 measurements were conducted using a saturation recovery pulse sequence. Relaxation curves were fit using Bruker Dynamics Center software and were found to be single component in nature. Density functional theory (DFT) calculations were performed using the projector augmented wave (PAW)^{13,14} potential as implemented in VASP code^{17,18} with following electrons treated explicitly: Al $3s^23p^1$, V $3s^23p^63d^34s^2$, Ga $4s^24p^13d^{10}$, P $3s^23p^3$, H $1s^1$, O $2s^22p^4$. A planewave kinetic energy cutoff of 500 eV and a Γ centered k-point Monkhorst Pack mesh¹⁹ with a density of 0.25 \AA^{-1} were chosen for all calculations. The PBE functional²⁰ was used and van der Waals forces were treated using the Tkatchenko-Scheffler scheme.²¹ **Ga system:** The α phase and δ high pressure phase of the Ga system were fully relaxed (atomic coordinates and unit cell shape) starting from experimental results until interatomic forces were less than 0.01 eV/\AA only with the constrain of their volume. Then the relaxed α phase and δ phase structures were further relaxed at different fixed volumes to obtain E - V relationship. These E - V values were used for the fitting of the Birch-Murnaghan equation of state:²²

$$E(V) = E_0 + \frac{9V_0B_0}{16} \left\{ \left[\left(\frac{V_0}{V} \right)^{\frac{2}{3}} - 1 \right]^3 B'_0 + \left[\left(\frac{V_0}{V} \right)^{\frac{2}{3}} - 1 \right]^2 \left[6 - 4 \left(\frac{V_0}{V} \right)^{\frac{2}{3}} \right] \right\} \quad (1)$$

Following parameters were obtained from the fitting: equilibrium volume (V_0), equilibrium bulk modulus (B_0) and the derivative of the bulk modulus with respect to external pressure (B'_0) as shown in Table S6. The external pressures in Figure S19 were calculated using the same equation of state in the pressure-volume expression:

$$P(V) = \frac{3B_0}{2} \left[\left(\frac{V_0}{V} \right)^{7/3} - \left(\frac{V_0}{V} \right)^{5/3} \right] \left\{ 1 + \frac{3}{4} (B'_0 - 4) \left[\left(\frac{V_0}{V} \right)^{2/3} - 1 \right] \right\} \quad (2)$$

Gibbs free energies of α and δ phases were calculated using the finite displacement method under the quasi-harmonic approximation (QHA) as implemented in the Phonopy code²³

by minimizing the following term by changing volume:

$$G(P, T) = \min_V \left[U(V) + F_{phonon}(T; V) + PV \right] \quad (3)$$

Due to the size of the unit cell $\approx 1400 \text{ \AA}^3$ (128 ions), only the single unit cell was used for calculations to reduce the computational expenses. Before phonon calculations, structures were further relaxed using an 800 eV cutoff until the interatomic forces smaller than 0.001 eV/Å. A $10 \times 10 \times 10$ Monkhorst Pack mesh¹⁹ is used for phonon density of states sampling. Vibrational entropies at different pressures and temperatures were calculated using:²⁴

$$S(P, T) = \int_0^T \frac{C_P(P, T')}{T'} dT' \quad (4)$$

, where C_P is the constant pressure heat capacity as given out by Phonopy. Pressure (volume) dependent bulk modulus were calculated using:

$$B = V \left(\frac{\partial^2 F}{\partial V^2} \right) \quad (5)$$

, where F is the Helmholtz free energy, and the external pressure can be obtained from volume using the equation of state above. The zero-point vibration energy (E_{ZP}) is evaluated by:

$$E_{ZP} = G - E_0 - PV \quad (6)$$

, where G is the Gibbs free energy and E_0 is the equilibrium ground state energy for equilibrium structure, PV term is 0 at ambient pressure.

DFT calculations for nuclear magnetic shift predictions were done using Vienna Ab initio Simulation Package (VASP).^{17,18} The generalized gradient approximation (GGA) Perdew-Burke-Ernzerhof (PBE) was utilized for structural relaxations and NMR parameter calculations.²⁰ Structural relaxations were performed from initial conditions obtained via XRD data with rigid cell parameters. A Γ -centered $3 \times 3 \times 3$ k-mesh was used to sample the Brillouin zone. The plane-wave basis set cut-off energy was set to 600 eV during relaxation calculations and 800 eV for NMR parameter calculations. NMR chemical shielding tensors were calculated using gauge included projector augmented wave (GIPAW) formalism.²⁵

Crystallographic information

All structures reported were solved via single crystal X-ray diffraction with relevant crystallographic data summarized in Tables S1 and S2. The CCDC deposition numbers are 1888648 – 1888652. One B alert was found for the reported β - $V(H_2PO_2)_3$.cif related to the wR_2 value of 0.42; a result from the twinned crystal that was used for structure solution. B alerts were also found in the two α phase systems related to the close packed nature of the oxygens surrounding the metal atom.

Table S1: Crystallographic data β -V(H₂PO₂)₃, α -Al(H₂PO₂)₃, and γ -Al(H₂PO₂)₃.

Empirical Formula	V(H ₂ PO ₂) ₃ (β)	Al(H ₂ PO ₂) ₃ (α)	Al(H ₂ PO ₂) ₃ (γ)
Crystal habit, color	plate, green	cube, clear	plate, clear
Crystal system	monoclinic	monoclinic	monoclinic
Space group (#)	$P2_1/c$ (14)	$P2_1/n$ (14)	C_2/c (15)
Volume (\AA^3)	764.7(1)	1454.9(2)	691.0(1)
T (K)	273	230	100
a (\AA)	11.922(8)	11.2333(7)	11.95(1)
b (\AA)	7.542(6)	11.5158(6)	7.809(8)
c (\AA)	8.860(6)	11.3670(5)	7.868(9)
α ($^\circ$)	90	90	90
β ($^\circ$)	106.29(2)	98.320(4)	109.77(2)
γ ($^\circ$)	90	90	90
Z	4	4	4
ρ (g mol ⁻¹)	245.90	443.88	221.94
Dens. (g cm ⁻³)	2.136	2.026	2.133
Abs. (mm ⁻¹)	1.898	0.911	0.960
F_{000}	488	896	448
Reflections (unique)	1215(691)	9237 (2566)	2843 (552)
R_{int}	0.2330	0.1232	0.0934
R_1	0.1509	0.0554	0.0462
wR_R	0.3856	0.1017	0.0784
∂F (e \AA^{-3})	1.423 & -1.600	0.530 & -0.812	0.587 & -0.502
GOF	1.095	1.002	0.973

Table S2: Crystallographic data α -Ga(H₂PO₂)₃ and δ -Ga(H₂PO₂)₃.

Empirical Formula	Ga(H ₂ PO ₂) ₃ (α)	Ga(H ₂ PO ₂) ₃ (δ)
Crystal habit, color	cube, clear	cube, clear
Crystal system	monoclinic	monoclinic
Space group (#)	$P2_1/n$ (14)	$P2_1/n$ (14)
Volume (Å ³)	1489.4(4)	1361.2(3)
T (K)	296(2)	293(2)
P (GPa)	0	1.33
a (Å)	11.293(2)	11.3584(6)
b (Å)	11.614(2)	11.1052(1)
c (Å)	11.482(2)	11.327(2)
α (°)	90	90
β (°)	98.547(4)	107.68(1)
γ (°)	90	90
Z	4	4
ρ (g mol ⁻¹)	529.36	529.36
Dens. (g cm ⁻³)	2.361	2.583
Abs. (mm ⁻¹)	4.312	1.044
F_{000}	1040	1040
Reflections (unique)	8720 (2801)	4568 (1925)
R_{int}	0.0961	0.0315
R_1	0.0464	0.0274
wR_R	0.0525	0.0697
∂F (eÅ ⁻³)	0.749 & -0.892	0.412 & -0.291
GOF	1.158	1.107

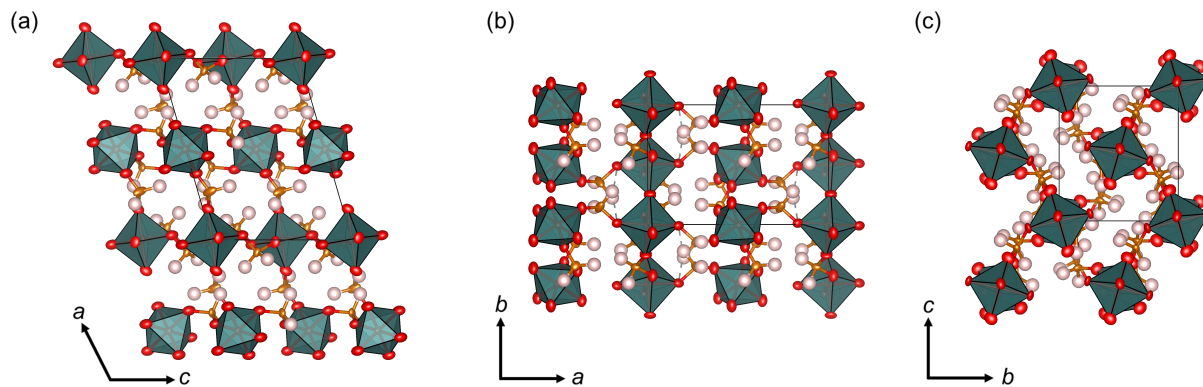


Figure S1: Views of $\beta\text{-V}(\text{H}_2\text{PO}_2)_3$ with 50% thermal ellipsoids.

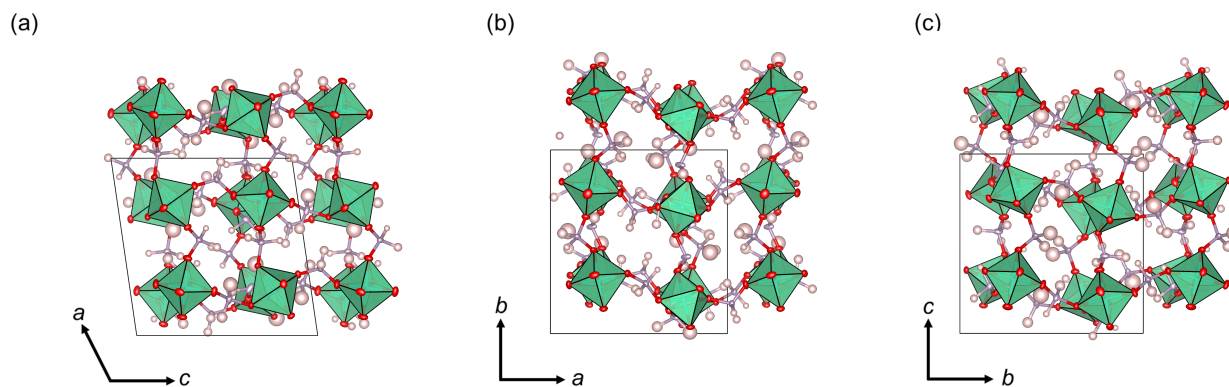


Figure S2: Views of $\alpha\text{-Al}(\text{H}_2\text{PO}_2)_3$ with 50% thermal ellipsoids.

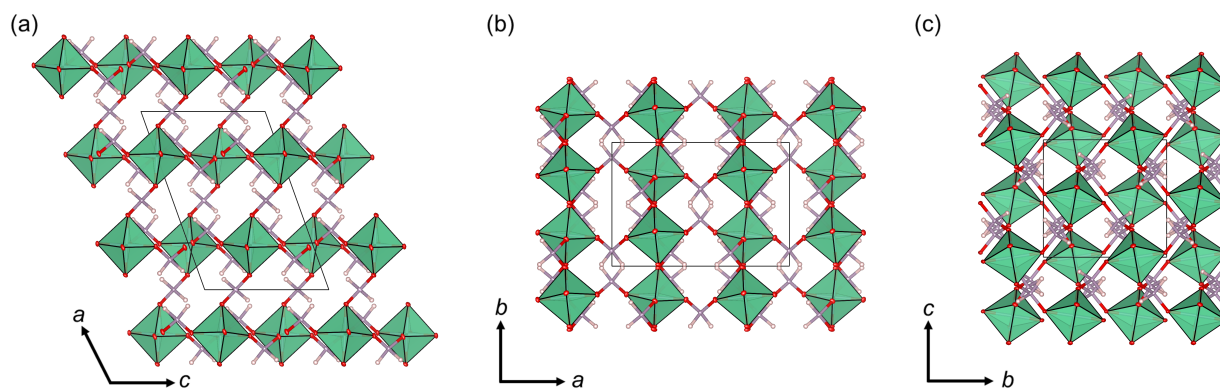


Figure S3: Views of $\gamma\text{-Al}(\text{H}_2\text{PO}_2)_3$ with 50% thermal ellipsoids.

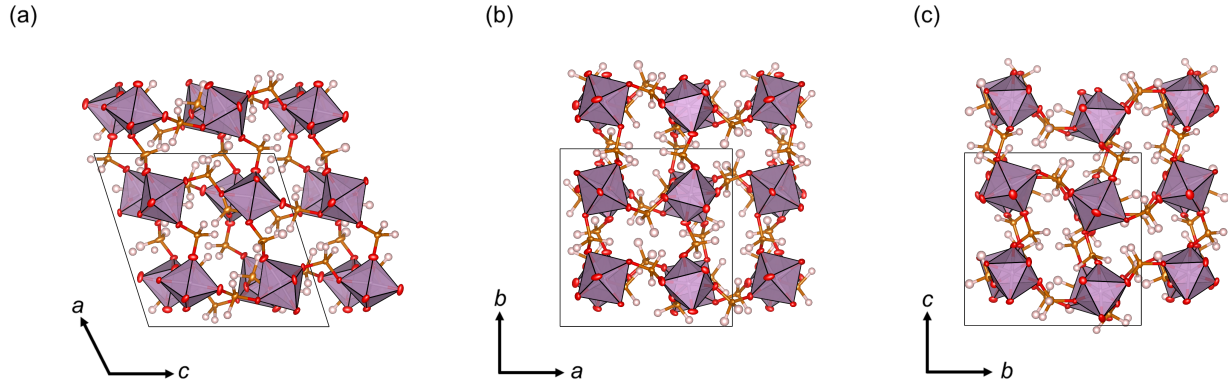


Figure S4: Views of $\delta\text{-Ga}(\text{H}_2\text{PO}_2)_3$ with 50% thermal elipsoids.

Expanded Glazer notation

Octahedral tilting and columnar shifts of the reported phases are assigned as described by Boström and co-workers,²⁶ and used in our previous paper on hypophosphite-based dense frameworks.²⁷ The method for assigning these tilts and shifts are summarised in the latter paper: “[the matrix notation for octahedral tilting and columnar shifts] extend Glazer’s widely used tilt notation to allow description of the additional correlation of distortions possible in perovskite analogues with polyatomic X ions. These are manifested as the rotation of octahedra (tilts) or the displacement of columns or planes of octahedra (shifts). Both tilt and shift descriptors each take the form of a 3×3 matrix. The diagonal terms in the tilt matrix can be determined by looking down the relevant pseudo-cubic axis and correspond to the normal Glazer terms. The off-diagonal terms are determined by taking slices of the structure. For example, in the bc plane, the correlation of rotations around a propagating in b and c give the off-diagonal terms of the first row. In perovskites with monoatomic X , the off-diagonal terms are constrained to be ‘-’ if tilts are active or ‘0’ if they are inactive. The full tilt matrix is constructed from generalised Glazer terms $g_{ij} = \epsilon_i \exp[2\pi i k_i j]$, with $\epsilon = (0,1)$ indicating whether a tilt is active, while k is the wavevector of the propagation. We draw attention to the periodicity of the tilt – most known perovskites, including hybrids, are either in phase $k = 0$, $g = 1$ [‘+’ by contention]) or out-of-phase

($k = 1/2$, $g = -1$ ['-' by convention]). For the hypophosphite systems, we see values of $-0.5 + \sqrt{3}/2i$ ($k = 1/3$), i ($k = 1/4$), and $0.5 + \sqrt{3}/2i$ ($k = 1/6$) – that is, periodicities of 3, 4 and even 6 octahedra. These periodicities do not uniquely describe patterns of rotation; for example, we see a variety of $k = 1/4$ tilts here. Shifts can likewise be assigned by considering slices of the structure. Each off-diagonal corresponds to the properties of a shift polarized along that axis. By convention, the diagonal terms are '+' if shifts are active in that axis or 0 if they are inactive; the remaining two terms correspond to the correlations in the two perpendicular directions.”

In Figures S5–S8, we show views for each $M(\text{H}_2\text{PO}_2)_3$ phase down a pseudocubic axes a , b , and c , and describe the tilt and shift patterns in terms of these axes rather than the crystallographic ones. The crystallographic axes relative to each pseudocubic axes are denoted at the bottom left hand corners of each panel. The magnitude of octahedral tilting in these systems is much higher than in the $AM(\text{H}_2\text{PO}_2)_3$ perovskites. We believe this to be related to the greater degree of structural rigidity provided by the A -site cations. The most pronounced examples of increased octahedral tilting are seen in the β - $\text{V}(\text{H}_2\text{PO}_2)_3$ and γ - $\text{Al}(\text{H}_2\text{PO}_2)_3$ compounds.

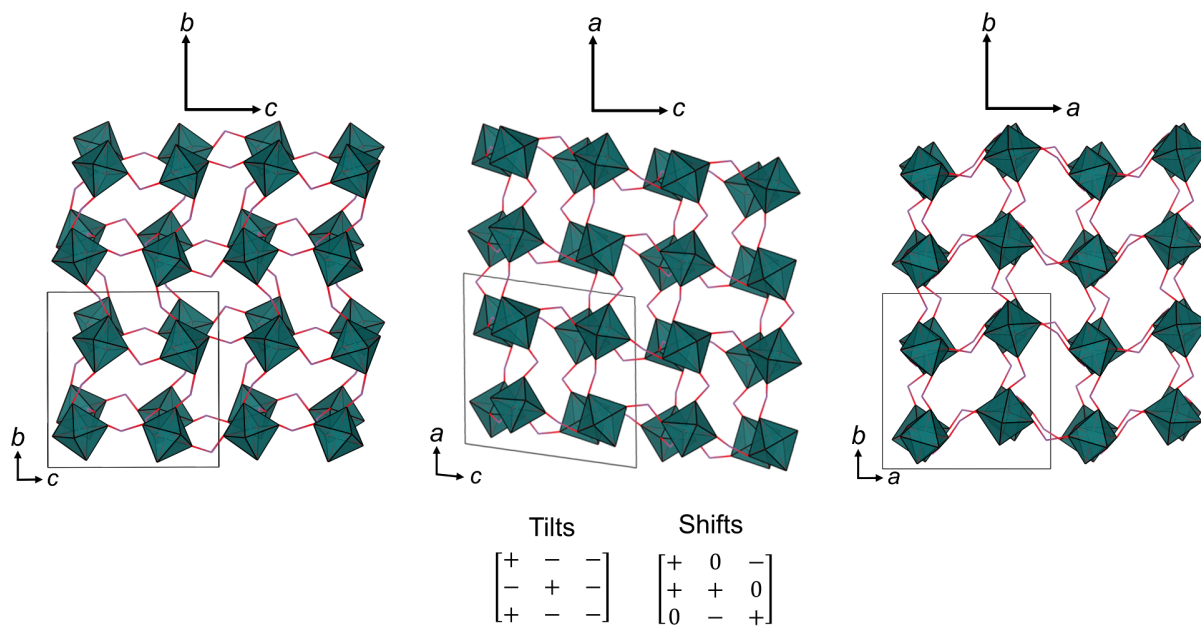


Figure S5: Views of the pseudocubic axes of α - $M(\text{H}_2\text{PO}_2)_3$ ($M = \text{V}, \text{Al}, \text{Ga}$, $P2_1/n$) and tilt and shift matrices.

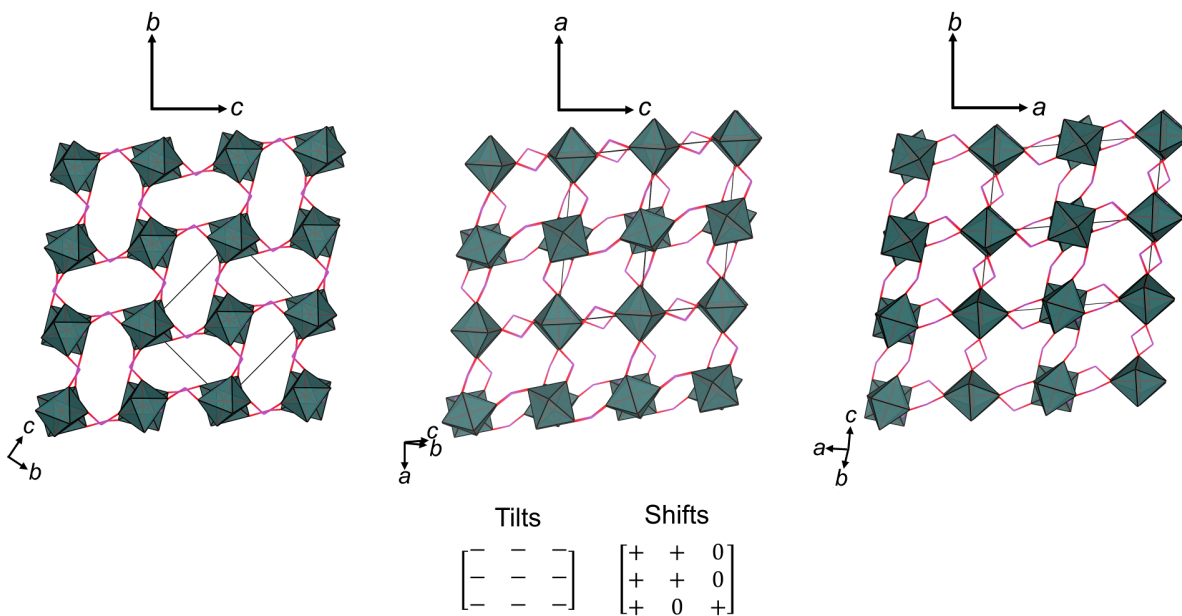


Figure S6: Views of the pseudocubic axes of β - $\text{V}(\text{H}_2\text{PO}_2)_3$ ($P2_1/c$) and tilt and shift matrices.

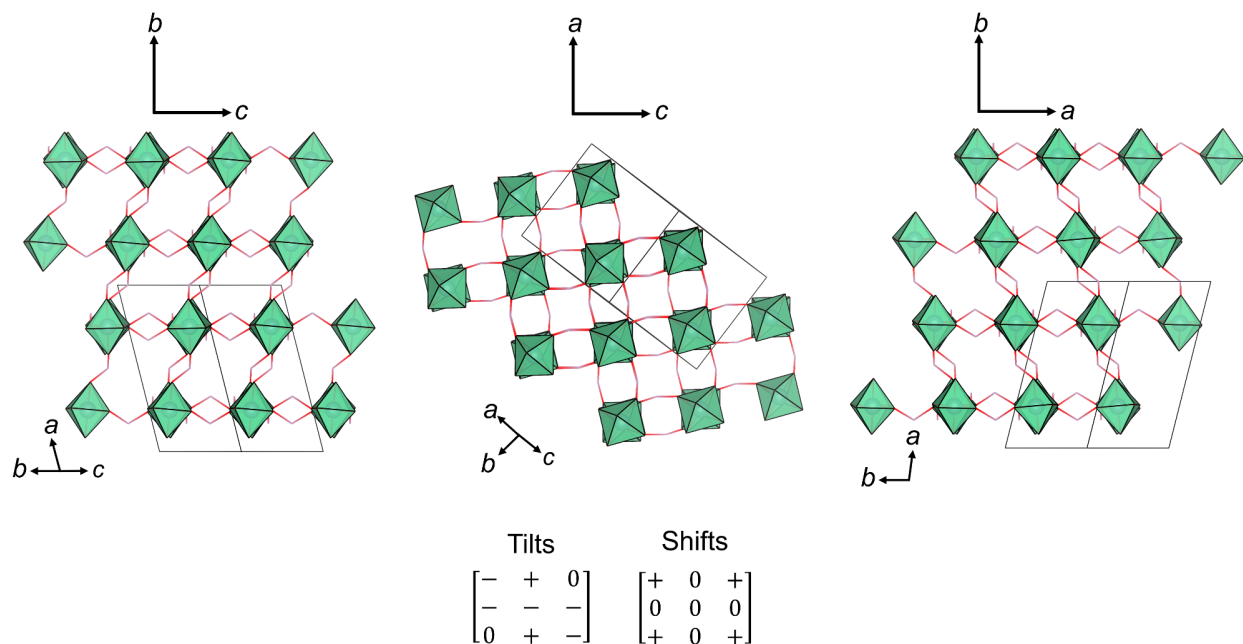


Figure S7: Views of the pseudocubic axes of $\gamma\text{-Al}(\text{H}_2\text{PO}_2)_3$ ($C2/c$) and tilt and shift matrices.

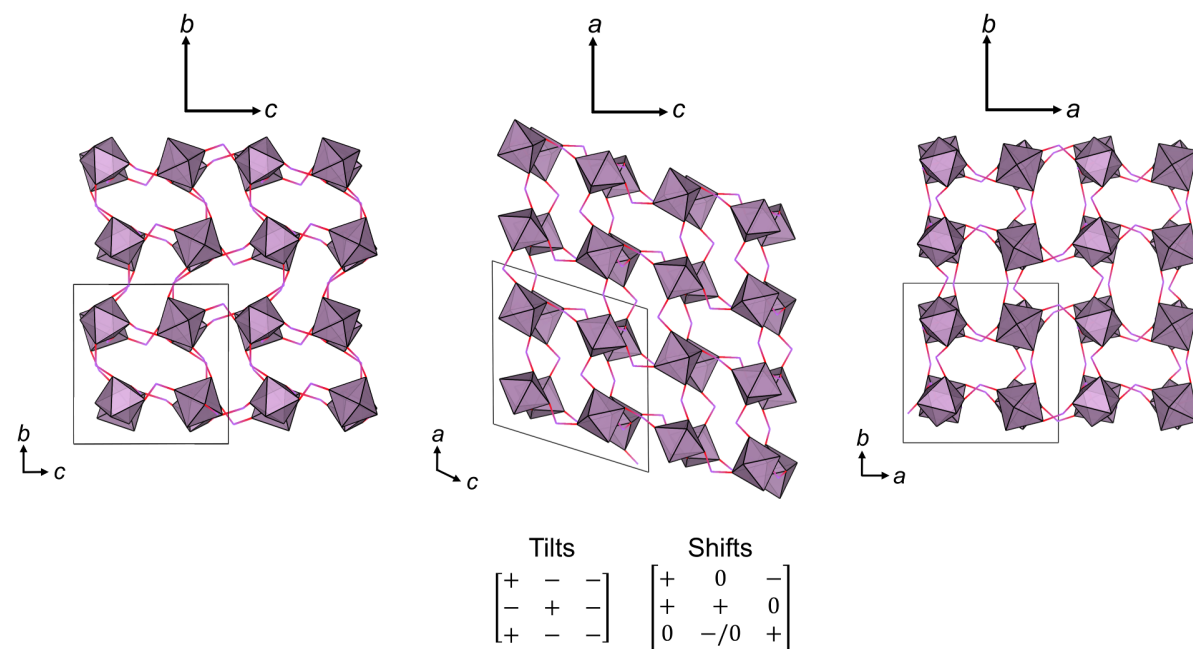


Figure S8: Views of the pseudocubic axes of $\delta\text{-Ga}(\text{H}_2\text{PO}_2)_3$ ($P2_1/n$) and tilt and shift matrices. The out-of-phase shift in the pseudocubic b direction in plane c is reduced in magnitude.

Powder X-ray diffraction

Single crystal structural models were used in Rietveld refinements against laboratory PXRD data; these are shown in Figures S9 - S12. Low temperature PXRD data for α -Ga(H₂PO₂)₃ compared to room temperature data is shown in Figure S13. The refinements indicate that the each bulk sample has unit cell parameters close to single crystal diffraction dimensions, with the refined lattice parameters listed in Table S3. We were unable to perform high temperature PXRD analysis on the β -V(H₂PO₂)₃ and γ -Al(H₂PO₂)₃ samples to look for any phase transitions on heating.

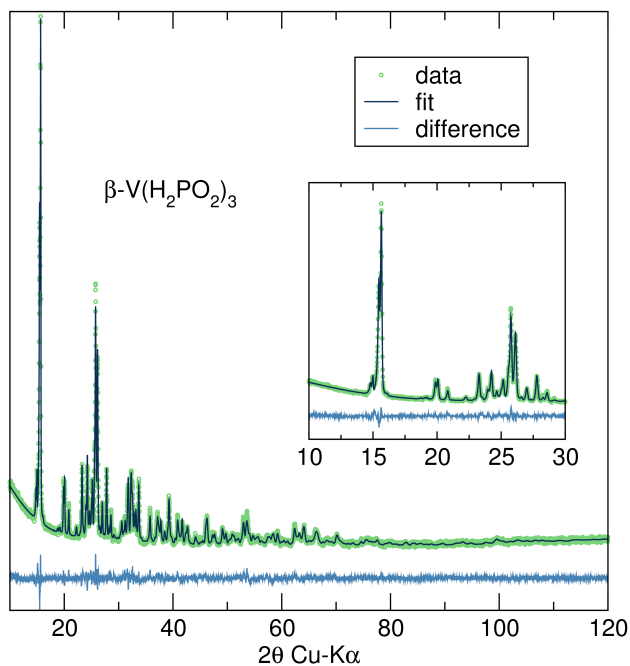


Figure S9: Rietveld refinement of β -V(H₂PO₂)₃

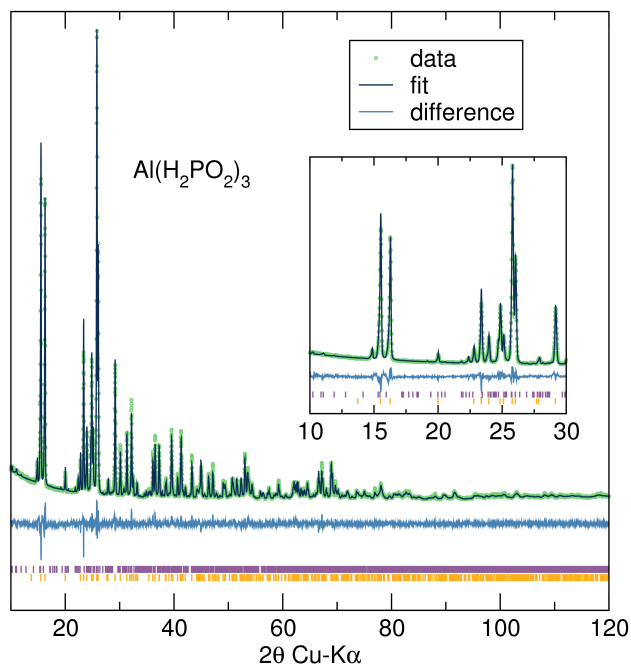


Figure S10: Rietveld refinement of reaction between $\text{Al}(\text{O-i-Pr})_3$ and H_3PO_2 which produces both $\gamma\text{-Al}(\text{H}_2\text{PO}_2)_3$ and $\alpha\text{-Al}(\text{H}_2\text{PO}_2)_3$. Orange ticks = γ , purple ticks = α . The patterns overlap, but indication of a multi-phase product can be noted by the additional peaks near $22^\circ 2\theta$ from the α phase. The α phase accounts for $\approx 10\%$ of the product.

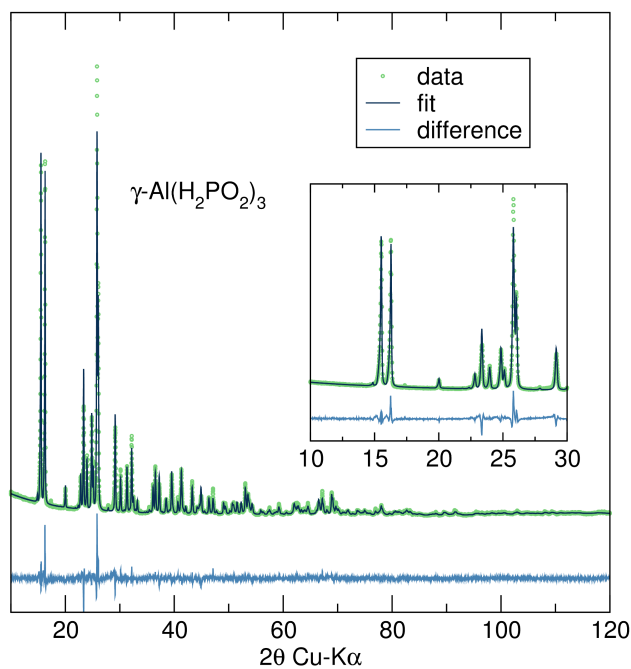


Figure S11: Rietveld refinement of $\gamma\text{-Al}(\text{H}_2\text{PO}_2)_3$, isolated phase pure by using $\gamma\text{-Al}_2\text{O}_3$ as the Al source.

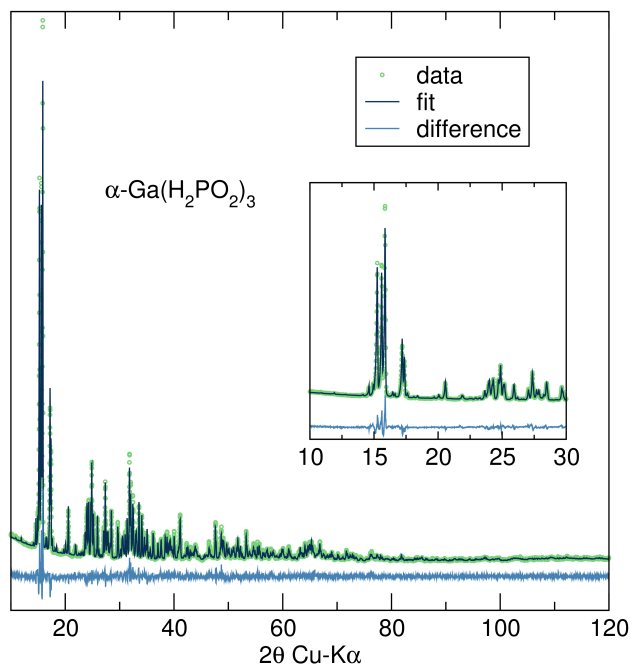


Figure S12: Rietveld refinement of $\alpha\text{-Ga}(\text{H}_2\text{PO}_2)_3$

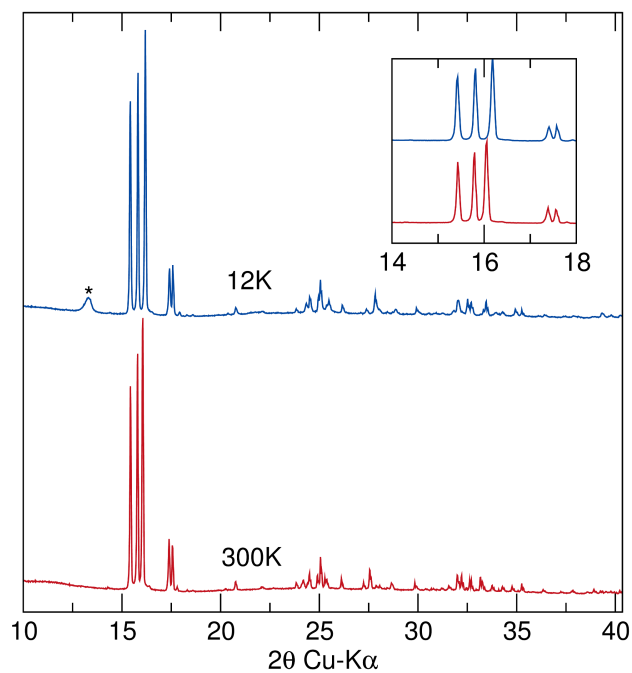


Figure S13: Comparison between 12 K and 300 K powder diffraction data of $\alpha\text{-Ga}(\text{H}_2\text{PO}_2)_3$, illustrating no first order phase transition. The starred peak at 13.5 2θ in the 12 K pattern is an artifact of the low temperature sample stage.

Table S3: Refined lattice parameters of samples that were obtained phase-pure.

Formula	V(H ₂ PO ₂) ₃ (β)	Al(H ₂ PO ₂) ₃ (γ)	Ga(H ₂ PO ₂) ₃ (α)
<i>a</i> (Å)	11.93	12.25	11.30
<i>b</i> (Å)	7.57	7.80	11.62
<i>c</i> (Å)	8.87	7.97	11.49
α (°)	90	90	90
β (°)	106.32	111.24	98.53
γ (°)	90	90	90

Nuclear magnetic resonance

Figures S14 and S15 show ¹H and ³¹P SPE spectra for α -Ga(H₂PO₂)₃, respectively. Only a single major component can be detected in the ¹H spectrum centered at 8 ppm. SCXRD indicates 12 distinct hydrogen sites, however strong dipole-dipole couplings between ¹H nuclei lead to broad NMR signals which can't be deconvoluted with the resolution available. An apparent minor impurity can be detected at approximately 2 ppm accounting for \approx 2% of the overall ¹H signal. Again, only a single major component can be seen in the ³¹P SPE spectrum, centered around 11 ppm. However, the insert depicts structure to the ³¹P peak.

To improve resolution, ¹H decoupling was used to reduce dipolar broadening and obtain a second ³¹P spectrum, as seen in Figure S16. Here, five components of the ³¹P spectrum can be simulated using Dmfit software.²⁸ The parameters of this simulated spectrum can be compared to DFT-GIPAW calculated ³¹P NMR parameters. Calculated NMR parameters, shown in Table S4, are corrected utilizing a scaling factor and reference shift:^{29,30}

$$\delta_{iso} = -k(\sigma_{iso} - \sigma_{ref})$$

Here, the scaling factor, *k*, was found to be 0.6027 with a reference shift, σ_{ref} , of 299.5 ppm.

Computed isotropic chemical shifts for the relaxed cell structure closely align with the simulated spectrum, allowing for peak assignments. It is apparent from the simulated

spectrum that two ^{31}P sites are represented within the deconvoluted peak centered at 9.0 ppm, corresponding to sites P1 and P3. Calculated chemical shifts for P1 and P3 are separated by less than 1 ppm, leaving their deconvolution beyond the resolution of the spectrum.

For ^{31}P nuclei, T_1 relaxation times are dictated mostly by intramolecular dipolar interactions and can be used to probe reorientational motion, as first described in theory by Bloembergen, Purcell, and Pound.³¹ Table S5 shows that the observed ^{31}P sites exhibit no significant difference in measured T_1 times.

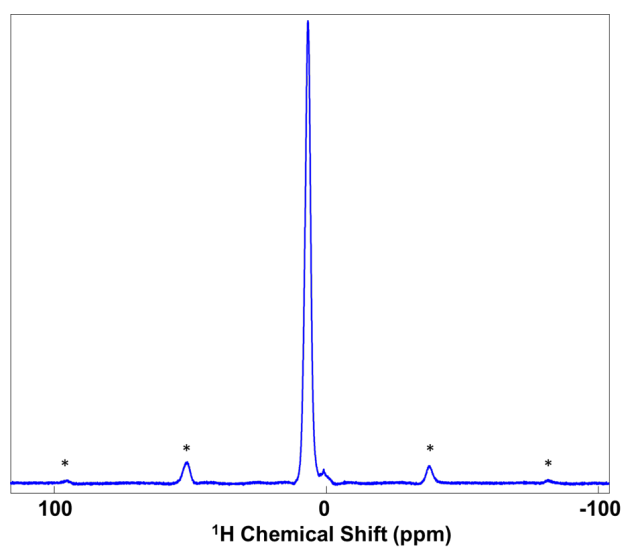


Figure S14: ^1H MAS SPE spectrum of $\alpha\text{-Ga}(\text{H}_2\text{PO}_2)_3$. Spinning sidebands are indicated by (*)

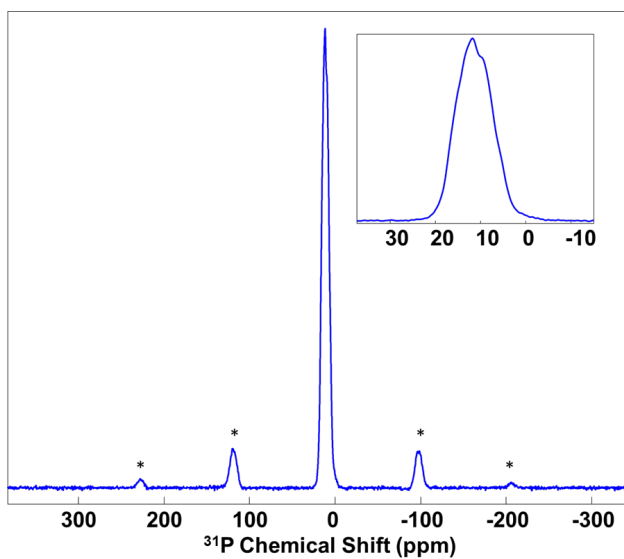


Figure S15: ^{31}P MAS SPE spectrum of $\alpha\text{-Ga}(\text{H}_2\text{PO}_2)_3$. Spinning sidebands indicated by (*)

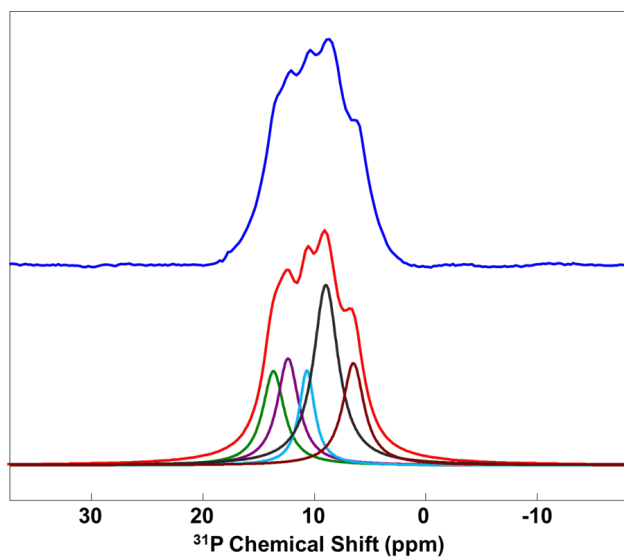


Figure S16: Experimental ^{31}P MAS spectrum with ^1H decoupling in blue for $\alpha\text{-Ga}(\text{H}_2\text{PO}_2)_3$. Simulated spectrum below, in red.

Table S4: Comparison of experimental ^{31}P spectrum with GIPAW calculated NMR parameters for $\alpha\text{-Ga}(\text{H}_2\text{PO}_2)_3$.

^{31}P Site	Exp Chem Shift (ppm)	GIPAW Chem Shift (ppm)	GIPAW Corrected (ppm)	Exp Intensity (%)
P4	6.5	-288.1	6.9	18
P1	9.0	-285.7	8.3	36
P3	-	-284.3	9.1	-
P2	10.7	-281.7	10.7	12
P5	12.4	-278.6	12.6	18
P6	13.7	-276.9	13.6	16

Table S5: T_1 relaxation times for five observed ^{31}P sites for $\alpha\text{-Ga}(\text{H}_2\text{PO}_2)_3$.

^{31}P site	T_1 (s)
P1/P3	134 ± 9
P2	136 ± 10
P4	132 ± 9
P5	135 ± 9
P6	135 ± 9

Thermogravimetric analysis (TGA)

Thermogravimetric analysis of the $M(\text{H}_2\text{PO}_2)_3$ compounds are presented in Figures S17–S18. Both materials show impressive stability, with minimal mass loss up until 900° .

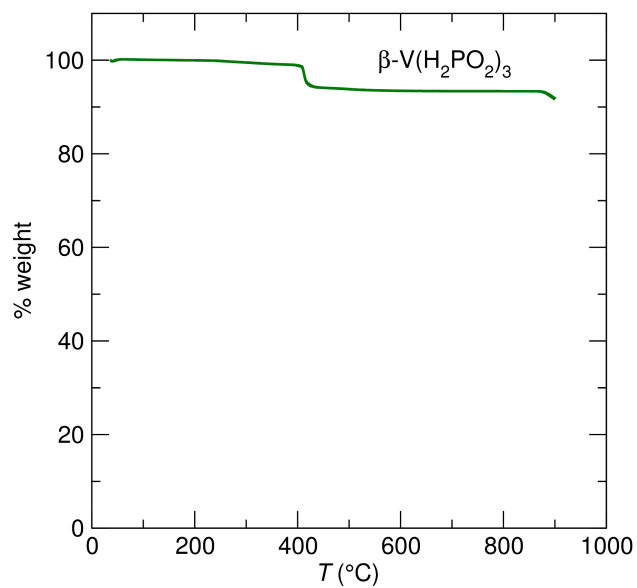


Figure S17: TGA of $\beta\text{-V}(\text{H}_2\text{PO}_2)_3$ from room temperature to 900°C.

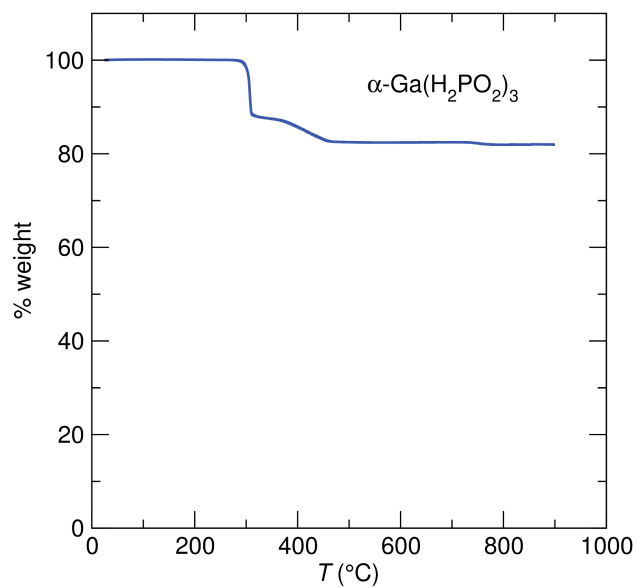


Figure S18: TGA of $\alpha\text{-Ga}(\text{H}_2\text{PO}_2)_3$ from room temperature to 900°C.

Density functional theory calculations

$\text{Ga}(\text{H}_2\text{PO}_2)_3$

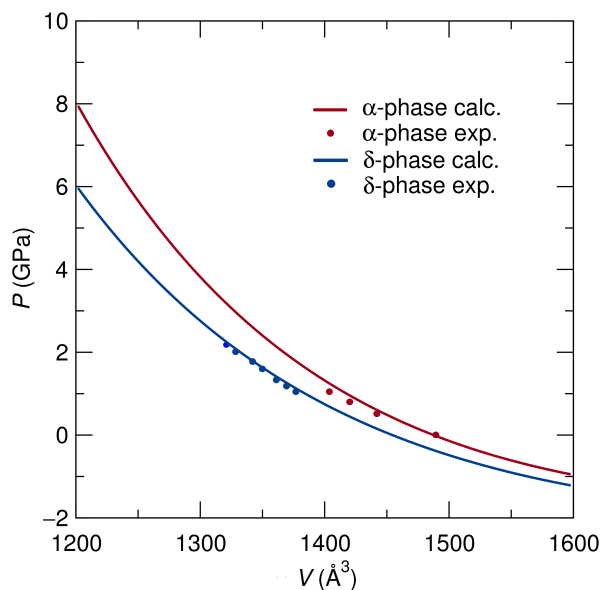


Figure S19: DFT external P vs. V plots of ambient pressure α -phase and high pressure δ phase for $\text{Ga}(\text{H}_2\text{PO}_2)_3$, as fitted from the Birch-Murnaghan equation of state (details in experimental information section). Points: experimental external P vs. V plots of α and δ phases.

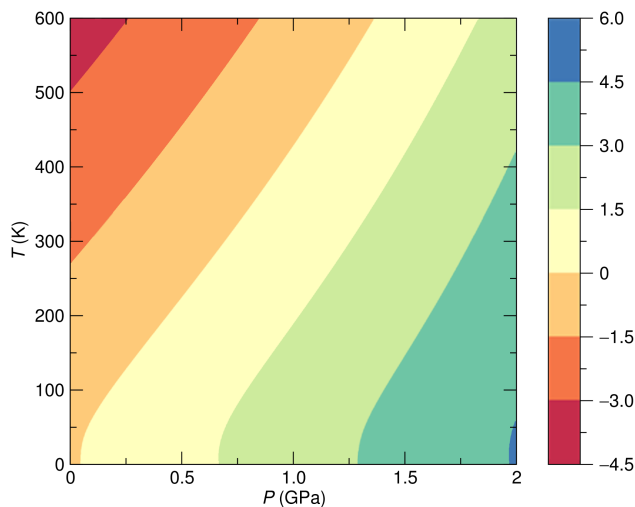


Figure S20: Gibbs free energy difference (α - δ) $\text{Ga}(\text{H}_2\text{PO}_2)_3$ (in kJ/mol *per f.u.*) as a function of T and P . Noted that there is no phase transition from the α to δ phase when decreasing temperature at 0 GPa due to the zero-point vibration.

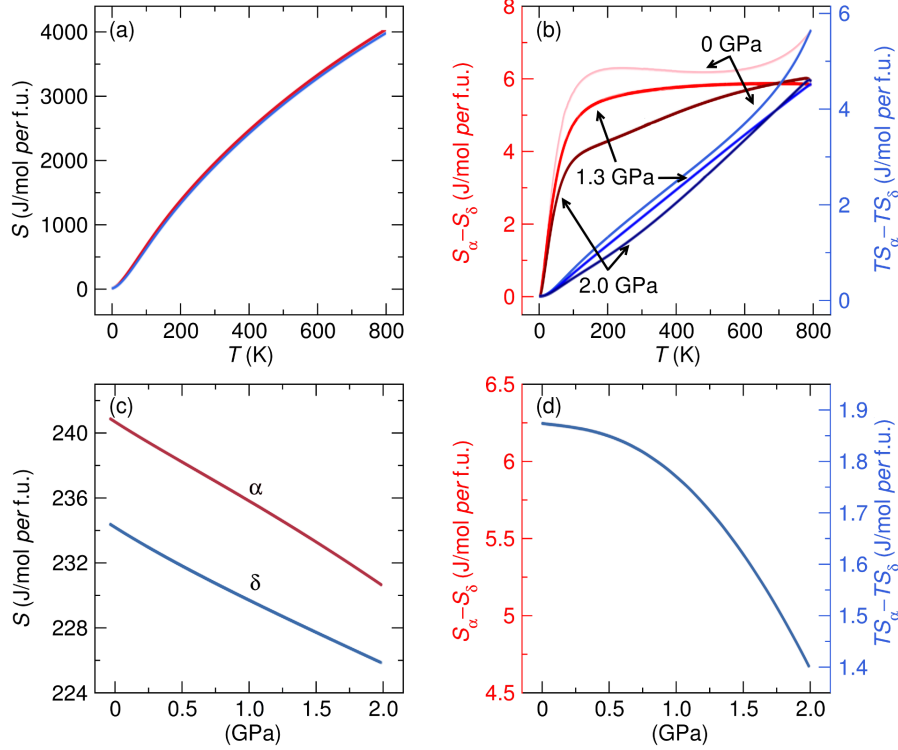


Figure S21: (a) Entropy (S) vs. temperature (T) plot of α (red) and δ (blue) and (b) their differences ($S_{\alpha}-S_{\delta}$) at 0 GPa, 1.3 GPa, and 2 GPa. (c) S vs. P plot of α (red) and HP (blue) and (d) their differences at 300 K.

Table S6: Comparison of DFT calculated lattice constants with experimental results for α -Ga(H₂PO₂)₃ phase.

	a (Å)	b (Å)	c (Å)	β (°)	V_0 (Å ³)
DFT	11.250	11.635	11.520	98.9	1489.8
Experiment	11.297	11.610	11.486	98.5	1489.9

Table S7: DFT calculated bulk modulus (B) at 300 K for α and β phases.

	α (at 0 GPa)	δ (at 1.3 GPa)
B (GPa)	16.70	24.77

Table S8: Calculated zero-point energy (E_{ZP}) (kJ/mol per f.u.) at ambient pressure for α - and δ -Ga(H₂PO₂)₃ phases

	α	δ
E_{ZP}	224.44	225.30

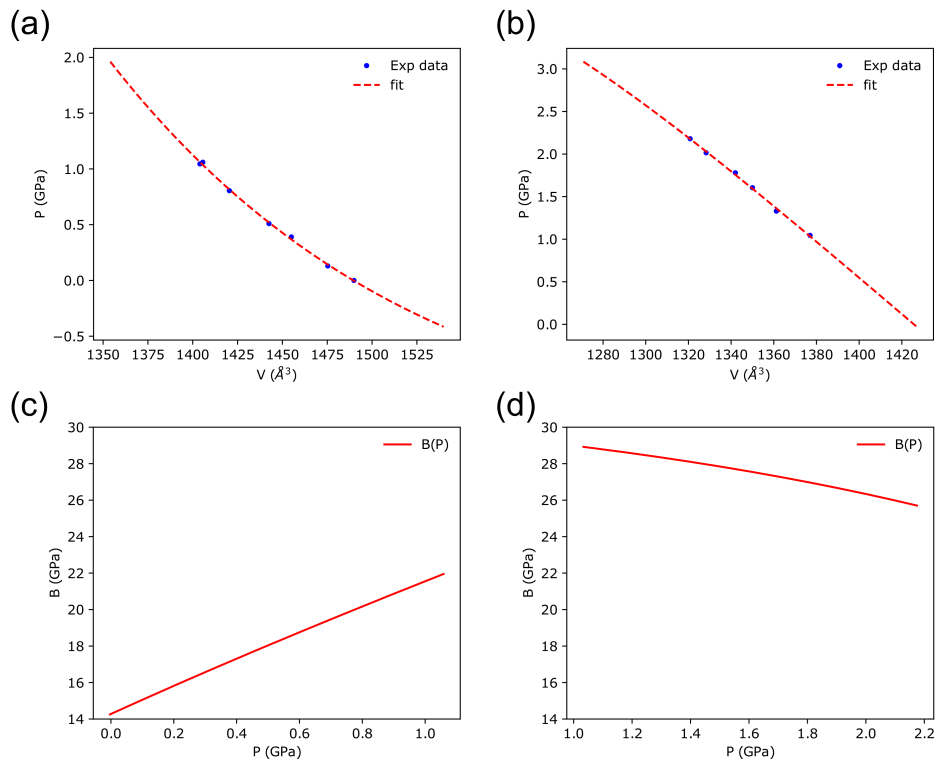


Figure S22: Birch-Murnaghan equation of state fits to experimental data for (a) α - $\text{Ga}(\text{H}_2\text{PO}_2)_3$ and (b) δ - $\text{Ga}(\text{H}_2\text{PO}_2)_3$. Calculated bulk modulus as pressure varies for (c) α - $\text{Ga}(\text{H}_2\text{PO}_2)_3$ and (d) δ - $\text{Ga}(\text{H}_2\text{PO}_2)_3$.

$\text{Al}(\text{H}_2\text{PO}_2)_3$

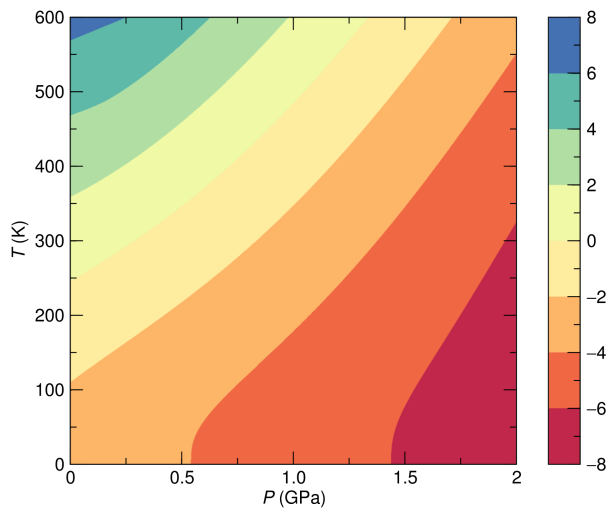


Figure S23: Gibbs free energy difference (α - γ) $\text{Al}(\text{H}_2\text{PO}_2)_3$ (in kJ/mol per f.u.) as a function of T and P .

$V(H_2PO_2)_3$

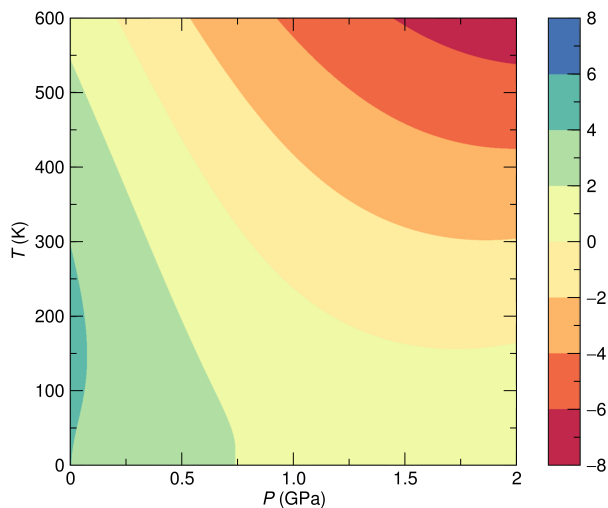


Figure S24: Gibbs free energy difference (α - β) $V(H_2PO_2)_3$ (in kJ/mol per f.u.) as a function of T and P .

References

- (1) H. A. Maouel, V. Alonzo, T. Roisnel, H. Rebbah and E. Le Fur, *Acta Cryst. C*, 2009, **65**, i36–i38.
- (2) SADABS; G. M. Sheldrick, University of Gottingen: Germany, 2005.
- (3) SHELXTL PC, Version 6.12; Bruker AXS Inc.: Madison, WI, 2005.
- (4) K. Momma and F. Izumi. *Commission on Crystallogr. Comput.* 2006, **7**, 106–119.
- (5) M. Merlini and M. Hanfland, *High Pressure Res.*, 2013, **33**, 511–522.
- (6) K. Yokogawa, K. Murata, H. Yoshino and S. Aoyama, *Jpn. J. Appl. Phys., Part 1*, 2007, **46**, 3636–3639.
- (7) *Rigaku Oxford Diffraction*, (2018), *CrysAlisPro Software system*, version 1.171.38.46, Rigaku Corporation, Oxford, UK.
- (8) G. M. Sheldrick, *Acta Crystallogr., Sect. C: Struct. Chem.*, 2015, **71**, 3–8.

- (9) G. M. Sheldrick, *Acta Crystallogr., Sect. A: Found. Adv.*, 2015, **71**, 3–8.
- (10) C. B. Hübschle, G. M. Sheldrick and B. Dittrich, *J. Appl. Crystallogr.*, 2011, **44**, 1281–1284.
- (11) C. F. Macrae, P. R. Edgington, P. McCabe, E. Pidcock, G. P. Shields, R. Taylor, M. Towler and J. van de Streek, *J. Appl. Cryst.* 2006, **39**, 453–457.
- (12) A. Coelho. *J. Appl. Cryst.* 2018, **51**, 210–218.
- (13) P. E. Blöchl, *Phys. Rev. B*, 1994, **50**, 17953–17979.
- (14) G. Kresse, *Phys. Rev. B* 1999, **59**, 1758–1775.
- (15) G. Kresse and J. Hafner, *Phys. Rev. B*, 1993, **47**, 558–561.
- (16) G. Kresse and J. Hafner, *Phys. Rev. B*, 1994, **49**, 14251–14269.
- (17) G. Kresse and J. Furthmüller, *Phys. Rev. B*, 1996, **54**, 11169–11186.
- (18) G. Kresse and J. Furthmüller, *Comput. Mater. Sci.*, 1996, **6**, 15–50.
- (19) H. J. Monkhorst and J. D. Pack, *Phys. Rev. B*, **1976**, *13*, 5188–5192.
- (20) J. P. Perdew, K. Burke and M. Ernzerhof, *Phys. Rev. Lett.*, 1997, **77**, 3865–3868.
- (21) A. Tkatchenko, M. Scheffler, *Phys. Rev. Lett.* 2009, **102**, 073005.
- (22) F. Birch, *Phys. Rev.* 1947, **71**, 809–824.
- (23) A. Togo, L. Chaput, I. Tanaka, G. Hug, *Phys. Rev. B* 2010, **81**, 174301.
- (24) D. C. Wallace, *Thermodynamics of Crystals*; Courier Corporation, 1998.
- (25) C. J. Pickard and F. Mauri, 2001, *Phys. Rev. B* **63**, 245101.
- (26) H. L. B. Boström, J. A. Hill, and A. L. Goodwin, *Phys. Chem. Chem. Phys.* 2016, **18**, 31881–31894.

- (27) Y. Wu, T. Binford, J. A. Hill, S. Shaker, J. Wang, and A. K. Cheetham, *Chem. Commun.* 2018, **54**, 3751–3754.
- (28) D. Massiot, D. 2002, *Magn. Reson. Chem.* **40**, 70–76.
- (29) A. Zheng, S. B. Liu, and F. Deng, *J. Phys. Chem. C* 2009, *113*, 15018–15023.
- (30) J. M. Griffin, J. R. Yates, A. J. Berry, S. Wimperis, and S. E. Ashbrook, *J. Am. Chem. Soc.* 2010, **132**, 15651–15660.
- (31) N. Bloembergen, E M. Purcell, and R. V. Pound, *Phys. Rev.* 1948, **73**, 679–712.